PAPER

Check for updates

Effect of fluorine substituents on benzothiadiazole-based D−π−A′−π−A photosensitizers for dye-sensitized solar cells†

Shuping Li, Xichuan Yang, ID * Li Zhang, Jincheng An, Bin Cai and XiuNa Wang

Two D−π−A′−π−A organic dyes with triazatruxene (TAT) as the electron donor, thiophene as the π-spacer, benzoic acid as the anchor group, and benzothiadiazole (BT) or difluorobenzo[c][1,2,5]thiadiazole (DFBT) as the additional acceptor, namely **LS101** and **LS102**, respectively, were applied to dye-sensitized solar cells (DSSCs). As fluorine substituents are usually strong electron-withdrawing groups, introducing two fluorine atoms into BT was expected to strengthen the electron-withdrawing ability of the auxiliary acceptor, resulting in DSSCs with a broader light capture region and further improved power conversion efficiency (PCE). Fluorine is the smallest electron-withdrawing group with an induction effect, but can also act as an electron-donating group owing to its conjugation effect. When the conjugation effect is dominant, the electron-withdrawing ability of additional acceptor DFBT decreases instead. Accordingly, the band gap of **LS102** was broadened and the UV-vis absorption spectrum was blue-shifted. In the end, DSSCs based on **LS101** achieved a champion PCE of 10.2% (J_{sc} = 15.1 mA cm^{-2}, V_{oc} = 966 mV, FF = 70.1%) while that based on **LS102** gave a PCE of only 8.6% (J_{sc} = 13.4 mA cm^{-2}, V_{oc} = 934 mV, FF = 69.1%) under standard AM 1.5G solar irradiation (100 mW cm^{-2}) with Co^{2+}/Co^{3+} as the electrolyte.

1. Introduction

Dye-sensitized solar cells (DSSCs) have attracted increasing attention over the past decades owing to their ease of fabrication, low production costs, flexibility in structural design and exceptional power conversion efficiency (PCE) even under indoor/diffused light-harvesting conditions.[1–8] Since first being reported in 1991, various photosensitizers have been synthesized, with the PCEs of DSSCs having increased up to 14%.[9–14] In contrast to metal dyes, in addition to a wide spectrum response and numerically appreciable molar extinction coefficient, organic photosensitizers also possess the advantages of facile synthesis and low cost.[15]

Donor−π-conjugation−acceptor (D−π−A) is a typical configuration of metal-free sensitizers, and is often considered as the formula for dye molecular structure design.[16] In our previous work, two triazatruxene (TAT)-based D−π−A sensitizers ZL001 and ZL003 were synthesized originally to obtain the best PCEs of 12.8% and 13.6%, respectively.[17] An additional π-bridge and acceptor can be introduced to broaden the ultraviolet-visible (UV-vis) absorption spectrum, which enhances the light-harvesting capability.[18,19] To obtain higher photoconversion

Institute of Artificial Photosynthesis, State Key Laboratory of Fine Chemicals, DUT-KTH Joint Education and Research Centre on Molecular Devices, Dalian University of Technology (DUT), 2 Linggong Rd, 116024 Dalian, China

† Electronic supplementary information (ESI) available. See DOI: 10.1039/c9ra09693k

efficiencies of DSSCs, we removed the triple bond to increase the rigidity and introduced two highly electronegative fluorine atoms into benzothiadiazole (BT) to access the stronger electron-withdrawing ability of the auxiliary acceptor based on ZL003 dye. Recently, difluorobenzo[c][1,2,5]thiadiazole (DFBT) has been a popular material in polymer solar cells,[20,21] because the small size of the two fluorine atoms is expected to minimize unacceptable steric interactions, while their strong electron affinity is desired to lower the lowest unoccupied molecular orbital (LUMO) energy levels and decrease the band gap.[22–26] Furthermore, the wise choice of solvents and additives can dramatically increase the short-circuit photocurrent density (J_{sc}) and fill factor (FF), which may be due to the fact that these fluorine atoms facilitate the optimized morphology of the film.[25,27–29] Fluorine-substituted benzothiadiazole has also proven to be an effective electron-accepting unit in small-molecule organic solar cells (SMOSCs).[30]

In this study, two D−π−A′−π−A photosensitizers **LS101** and **LS102** (Fig. 1) were synthesized with TAT as electron donor, thiophene as π-spacer, benzoic acid as anchor group, BT and DFBT as additional acceptors, respectively. DFBT was introduced to optimize the energy levels and widen the absorption spectrum response range. However, contrary to the desired result, the device containing **LS102** exhibited a lower J_{sc} and PCE. Various tests were conducted to determine the influence of fluorine on DFBT and explain the poorer photovoltaic performance of **LS102**-based DSSCs. We discovered that with respect to the induction effect and conjugation effect, fluorine atoms act as electron-
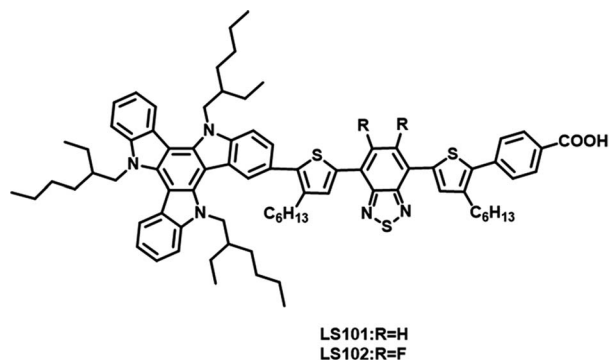
LS101:R=H
LS102:R=F

Fig. 1 Structures of dyes **LS101** and **LS102**.

withdrawing and electron-donating groups, respectively. The electron-withdrawing ability of additional DFBT was impaired when the conjugation effect was dominant over the induction effect. Consequently, the band gap of **LS102** was broadened and the UV-vis absorption spectrum was blue-shifted, resulting in a lower J_{sc}.

2. Experimental section

2.1 Synthesis

The particulars of the synthetic procedures are given in the ESI.†

2.2 Solar cell fabrication

Initially, the fluorine-doped tin oxide FTO (Pilkington, 2.2 mm thick, 15 ohm square) glass plates were cleaned by sonication in soap solution, deionized water, acetone and isopropanol consecutively. Then the substrates were blown with a hair dryer and treated with UV–O₃. In order to attach two dense layers to the FTO conductive glass, the substrates needed to be treated with 40 mM $TiCl_4$ aqueous solution at 70 °C for 45 minutes, then dried by deionized water and cleaned with UV–O₃. Next, the substrates were transferred to the muffle furnace and heated up to 500 °C in 3 h, then held for 1 h. After the temperature drops to 25 °C, the 4×4 mm² nanocrystalline porous TiO_2 transparent layer was then coated with TiO_2 paste by screen printing. TPP200 was printed as a scatting layer. Then the nanoporous TiO_2 electrodes were baked in the muffle furnace as before. After sintered photoanodes were cooled to 25 °C, they were immersed in dye bath (2×10^{-4} M in CH_2Cl_2) for 12 h. The substrates to which the dye was adsorbed served as the working electrode, Pt as the counter electrode, and the two portions were adhered by a hot-melt Surlyn film. Finally, the electrolyte is drilled into the sandwich by vacuum pump.

3. Results and discussion

3.1 Optical properties and electrochemical characterization

UV-vis absorption spectra of **LS101** and **LS102** dyes dissolved in CH_2Cl_2 solution (1×10^{-5} M) and adsorbed on TiO_2 film are shown in Fig. 2. Table 1 shows the corresponding parameters. Compared with **LS101**, the maximum absorption wavelength (λ_{max}) of **LS102** was blue-shifted from 505 to 486 nm, while the molar extinction coefficient (ε_{max}) was increased from 16 462 to 19 625 M^{-1} cm^{-1}. As expected, introducing fluorine atoms increased the spectral absorption intensity, but the change in
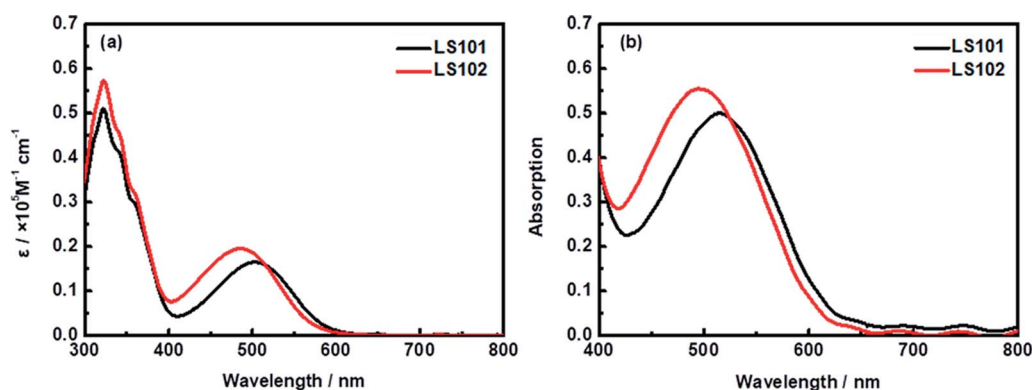

Fig. 2 Absorption spectra of dyes **LS101** and **LS102** (a) in CH_2Cl_2 solution and (b) on TiO_2 film.

Table 1 Optical and electrochemical data of the **LS101** and **LS102** dyes

Dye	$\lambda_{max}{}^a$ in DCM (nm)	ε (M^{-1} cm^{-1})	$\lambda_{max}{}^b$ on TiO_2 (nm)	$E_{0-0}{}^c$ (eV)	$E_{HOMO}{}^d$ (V)	$E_{LUMO}{}^e$ (V)	E_{HOMO} (V) (DFT)	E_{LUMO} (V) (DFT)
LS101	505	16 462	516	1.89	0.78	−1.11	0.68	−1.46
LS102	486	19 625	495	1.91	0.77	−1.14	0.67	−1.57

[a] Absorption maxima of dye **LS101** and **LS102** in CH_2Cl_2 solutions (1×10^{-5} M). [b] Absorption on TiO_2 film (electrolyte: 0.1 M TFSILi and 0.85 M TBP in CH_3CN). [c] $E_{0-0} = 1240/\lambda_{ea}$, λ_{ea} is the intersection of the tangent absorption wavelength on TiO_2 film with x-axis. [d] E_{HOMO} was recorded in DCM (Fc/Fc⁺ as an internal reference; potentials were converted to normal hydrogen electrode (NHE) by addition of 0.44 V (ref. 31)). [e] $E_{LUMO} = E_{HOMO} - E_{0-0}$.

the spectral absorption range was contrary to the desired effect. When two hydrogen atoms on benzothiadiazole were substituted with highly electronegative fluorine atoms, the electron-withdrawing ability of the additional acceptor should theoretically have been enhanced. However, the results were quite different owing to the electron-donating property resulting from the conjugation effect of fluorine atoms. The effect was exemplified by the blueshift of the UV-vis absorption spectrum of **LS102** in comparison to that of **LS101**. From Fig. 2b, when the photosensitizers were adsorbed on TiO_2 film, absorption peaks of two dyes were both slightly widened and bathochromic with respect to those in CH_2Cl_2 solution. The extension of the

absorption profile indicated that **LS101** and **LS102** were present on the TiO_2 film in a *J*-aggregation state,[32] which aided adequate light capture.

Cyclic voltammetry (CV) measurements were performed in CH_2Cl_2 solution (Fig. 3 and Table 1) to investigate the electrochemical properties of the two photosensitizers. For donor segments with the identical structures, the first oxidation potentials corresponding to the highest occupied molecular orbital (HOMO) energy levels of **LS101** and **LS102** were almost the same, at 0.78 and 0.77 V *vs.* NHE, respectively. These values were more positive than that of $Co(bpy)_3^{2+/3+}$ (0.56 V *vs.* NHE, bpy = 2,2′-bipyridine), ensuring the driving force accessible for
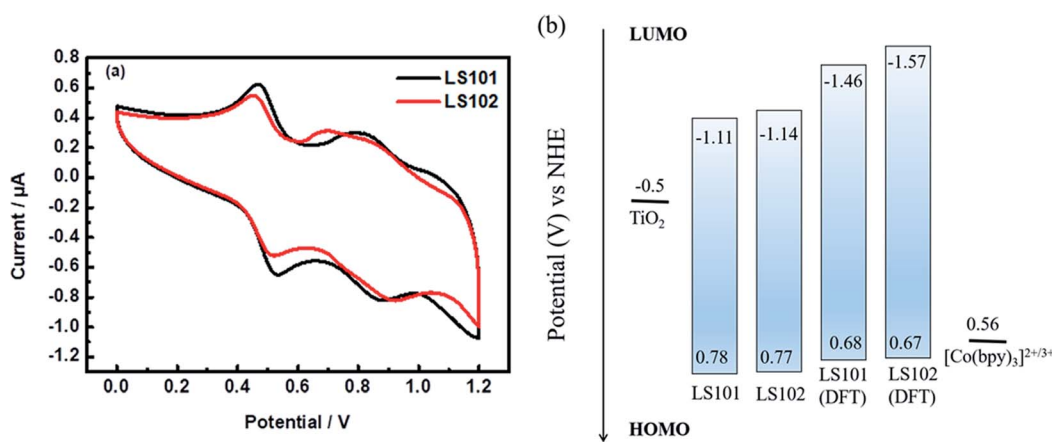

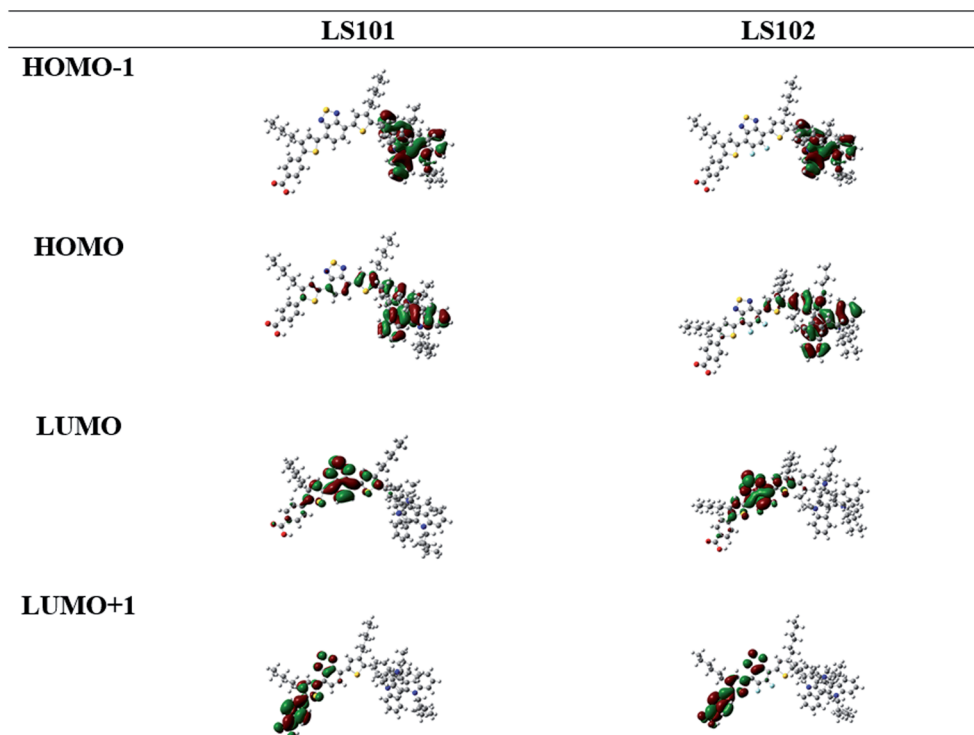Fig. 3 (a) Cyclic voltammetry curves of dyes **LS101** and **LS102** (b) HOMO and LUMO energy levels.

Fig. 4 Calculated frontier orbitals of dyes **LS101** and **LS102**.

dye regeneration. The band gap energies (E_{0-0}) of **LS101** and **LS102** were estimated as 1.89 and 1.91 eV, respectively. The LUMO energy levels were −1.11 and −1.14 V *vs.* NHE for **LS101** and **LS102**. The LUMO energy levels of the two dyes were more negative than the Fermi level of TiO_2 (−0.5 V *vs.* NHE), ensuring the sufficient driving force for the progress of electron injection. Since the electron-donating ability of the fluorine atoms in the conjugation effect exceeded the electron-withdrawing ability on the inductive effect, it dominated, making the electron-withdrawing ability of additional acceptor DFBT weakened. Therefore, the LUMO energy level of **LS102** was more negative and its band gap was broader.

3.2 Theoretical calculation

To better understand the molecular geometry and performance of **LS101** and **LS102** dyes, density functional theory (DFT) calculations were conducted using the Gaussian 09 program package at the B3LYP/6-311G (d, p) level. The calculated frontier molecular orbitals of dyes **LS101** and **LS102** are shown in Fig. 4. HOMOs of two dyes were mostly distributed on the TAT moiety and thiophene, while the HOMO−1 levels were predominantly located on the TAT donor. LUMOs were mostly delocalized on BT and DFBT, while the LUMO+1 levels were primarily located on the benzoic acid anchor group. Successful electron migration from HOMO to LUMO ensured successive charge separation and electron injection into the conduction band of TiO_2.[33] The HOMO, LUMO and E_{0-0} from DFT calculations were consistent with the values from the test (see Table 1 and Fig. 3b), with the E_{0-0} of **LS102** found to be larger than that of

LS101. This indicated that the conjugation effect of fluorine increased the LUMO level and blue-shifted its UV-vis spectrum.

As we know, the conjugation effect was caused by the sp^2 orbit of F atom which conjugated with overall conjugation system and donated its electron to the system. From the LUMO orbit of **LS101** and **LS102** (the partial enlarged orbitals were put in Fig. S1†), we can observe that the electron wave function was located on F atom in **LS102**, but there was no distribution of electron wave function on the corresponding H atom in **LS101**. The induction effect can be explained by the calculated dipole moments, **LS101** and **LS102** giving 7.2983 debye and 7.4563 debye respectively. With the same electron donating moiety, **LS102** containing F atom on the electron withdrawing moiety gave larger dipole moment than that of **LS101** containing no F atom, which meant that F atom gave electron withdrawing induction effect. The above DFT calculations successfully explained that the fluorine atom did have both the conjugation effect as the electron donor and the induction effect as electron-withdrawing group. From the UV-vis absorption spectra, the maximum absorption wavelength of **LS102** was blue-shifted comparing with **LS101**, which illustrated the electron-withdrawing ability of DFBT was weaker than BT, so the conjugation effect was dominant.

3.3 Photovoltaic performances

To investigate the photovoltaic properties of dyes **LS101** and **LS102** in DSSCs, the photocurrent density–voltage (*J–V*) characteristics were measured (Fig. 5a) with the device parameters shown in Table 2. Under standard global AM1.5 solar
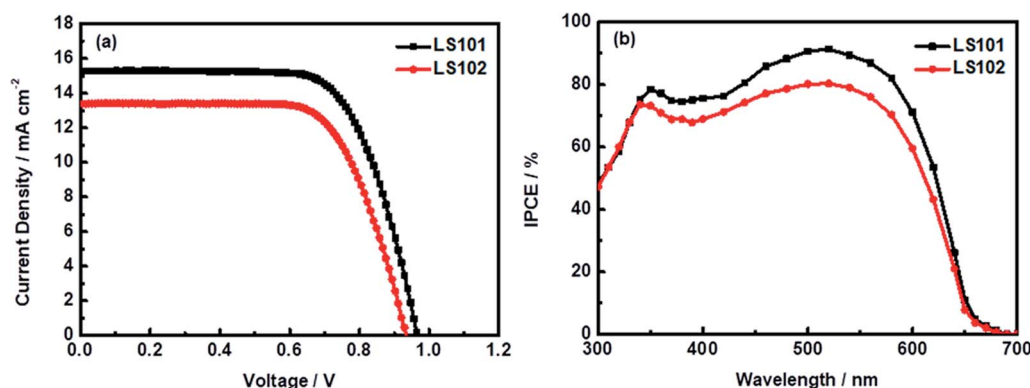

Fig. 5 (a) Current density–voltage properties for DSSCs measured under simulated AM 1.5G illumination (b) IPCE spectra for DSSCs based on **LS101** and **LS102**.

Table 2 Photovoltaic parameters of the DSSCs based on dyes **LS101** and **LS102**[a]

Dye[b]	V_{oc} (mV)	J_{sc} (mA cm^{-2})	FF (%)	PCE (%)	DL[c] (×10^{-8} mol cm^{-2})
LS101	966	15.1	70.1	10.2	9.3
LS102	934	13.4	69.1	8.6	6.5

[a] Photovoltaic performance under AM1.5 irradiation (100 mW cm^{-2}) of the DSSCs containing **LS101** and **LS102** dyes. Active area of the devices is 0.16 cm^{-2}. The cobalt-based electrolyte consists of 0.22 M [Co(bpy)$_3$](TFSI)$_2$, 0.05 M [Co(bpy)$_3$](TFSI)$_3$, 0.1 M TFSILi, and 0.85 M TBP in acetonitrile. [b] Dye bath: 2 × 10^{-4} M in CH$_2$Cl$_2$. [c] DL means the dye loading capacity on the mesoscopic TiO$_2$ film for DSSCs.
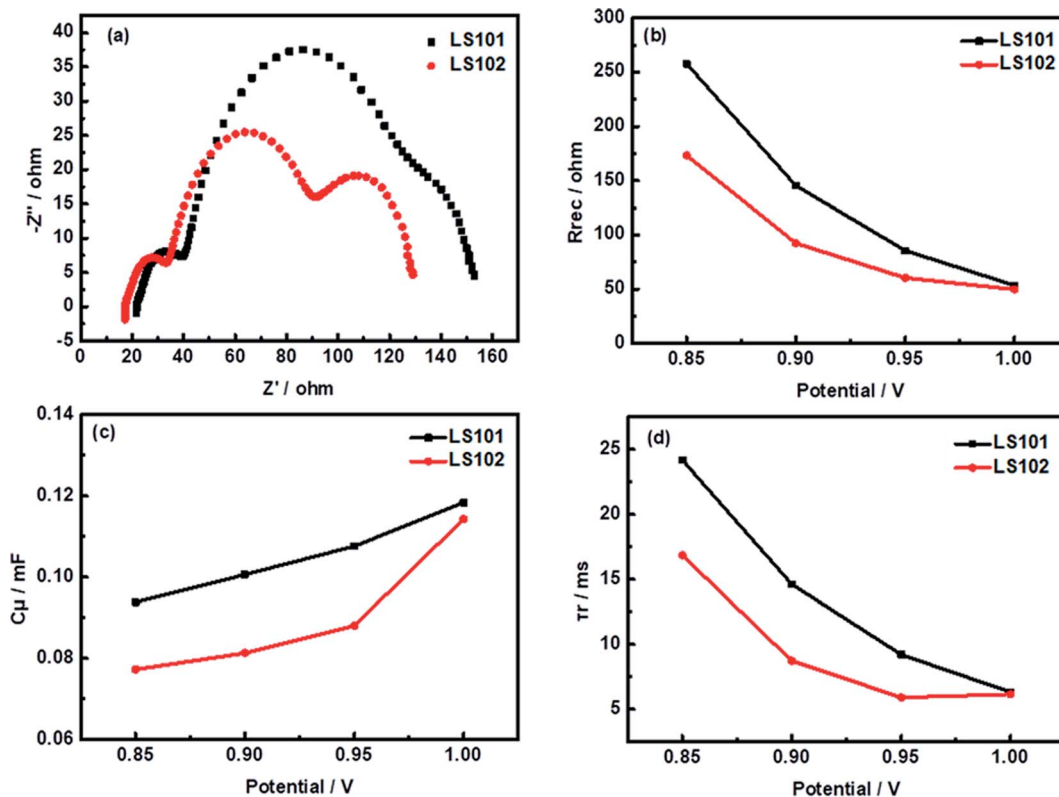
Fig. 6 Impedance analysis: (a) Nyquist plots under forward bias of −950 mV (b) recombination resistance R_{rec} (c) chemical capacitance C_μ (d) calculated electron lifetime τ_r.

irradiation (100 mW cm^{-2}), the **LS101**-sensitized cell showed a higher PCE of 10.2% with a J_{sc} of 15.1 mA cm^{-2}, V_{oc} of 966 mV, and FF of 70.1%. Under the same experiment conditions, DSSCs based on **LS102** exhibited a lower PCE of 8.6% (J_{sc} = 13.4 mA cm^{-2}, V_{oc} = 934 mV, FF = 69.1%). Dye loading capacity measurements were conducted to evaluate the strength of the dye–TiO$_2$ interaction. From Table 2, **LS101** showed a dye loading of 9.3×10^{-8} mol cm^{-2} compared with 6.5×10^{-8} mol cm^{-2} for **LS102**. Generally, a larger dye loading amount results in devices with a stronger light harvesting ability, which considerably affects the photocurrent. The dye loading measurements on TiO$_2$ are provided in the ESI.† The devices based on **LS101** showed a higher J_{sc} benefiting from the wide UV-vis absorption spectra (Fig. 2) and a high dye loading capacity, which compensated the disadvantageous impact of the lower molar extinction coefficient.

To further verify the origin of the different J_{sc} values, the incident photon-to-current conversion efficiency (IPCE) spectrum was measured. As shown in Fig. 5b, the IPCE spectra of DSSCs based on **LS101** and **LS102** were both mainly observed in the wavelength range of 350–600 nm. However, the peak intensities of DSSCs containing **LS101** were generally higher than those containing **LS102**, which contributed to the enhanced photocurrent. The maximum peak value was 91% for the device based on **LS101**, in contrast to that of the device based on **LS102**, which was only 80% at 520 nm. This trend roughly corresponded to the increase in current density.

To explore the factors affecting the differences of the V_{oc} between devices based on **LS101** and **LS102**, typical electrochemical impedance spectroscopy (EIS) experiments were conducted. Some relevant data are shown in Fig. 6, with specific values under −0.95 V shown in Table 3.

Using the same electrolyte, the V_{oc} could be directly related to the position of the TiO$_2$ conduction band (E_{cb}). When different dyes were adsorbed onto TiO$_2$, its quasi-Fermi energy level will change by varying degrees. To evaluate this shift, charge transport resistance (R_{tr}) at Pt/electrolyte interface, electron recombination resistance (R_{rec}) at the TiO$_2$/dye/ electrolyte interfaces, Warburg diffusion processes (Co^{2+}/Co^{3+}) in the electrolyte, and chemical capacitance (C_μ) responses have been fitted with an equivalent circuit model (Fig. S3†).[34–36] The resulting Nyquist plots of solar cells based on the two dyes are shown in Fig. 6a. As the same platinum electrode and electrolyte were used in the two systems, the left semicircles at high

Table 3 EIS parameters[a] for DSSCs based on **LS101** and **LS102** dyes

Dye	R_{tr} (Ω)	R_{rec} (Ω)	C_μ (mF)	τ_r (ms)	η_{cc} (%)
LS101	18.21	85.58	0.11	9.21	82.5
LS102	16.08	60.34	0.09	5.42	79.0

[a] Calculated value from EIS data measured at a forward bias of −950 mV under dark conditions. R_{tr}: transport resistance, R_{rec}: charge recombination resistance, C_μ: chemical capacitance, τ_r: electron lifetime, η_{cc}: charge-collection efficiency.

frequency corresponding to R_{tr} were similar. The second semicircle located in the middle-frequency region represented R_{rec} with the **LS102** device showing a much smaller semicircle than **LS101**. This suggested that more serious charge recombination between injected electron and redox couple of the photoanode interface occurred in the **LS102**-based device under dark conditions.[37] The R_{rec} values of **LS101** and **LS102** are 85.58 Ω and 60.34 Ω, respectively, at a forward bias of −950 mV (Table 3). The order of fitted R_{rec} values was consistent with the trend in the V_{oc} values of **LS101** and **LS102**. The semicircle in the low frequency region represented the impedance of the diffusion process. Since the electrolyte formulations used by the two devices based on **LS101** and **LS102** were exactly the same, this data had no significant difference. As shown in Fig. 6c, the C_μ responses of the DSSCs increased in the order **LS101** > **LS102**, indicating a more negative shift in E_{cb} when **LS101** was adsorbed on the TiO_2 surface compared with **LS102**.[38] This might account for the lower V_{oc} of the **LS102** device to a certain extent. Furthermore, Fig. 6d shows the electron lifetimes for the two dyes which were estimated using the equation ($\tau_r = R_{rec} \times C_\mu$). A longer electron lifetime corresponds to a higher electron density in the TiO_2 conduction band and a lower charge recombination rate, resulting in a higher V_{oc}.[39] The corresponding low V_{oc} of **LS102**, which had a shorter electronic lifetime confirms this statement. The charge collection efficiency was calculated using the formula $\eta_{cc} = R_{rec} \times (R_{rec} + R_{tr})^{-1}$. The η_{cc} value of **LS101** was 82.5%, while that of **LS102** was 79.0%, which showed that the injected electrons could be extracted more effectively in **LS101**, reflecting its better photovoltaic performance.[40]

4. Conclusion

In summary, we successfully introduced two D−π−A′−π−A organic sensitizers **LS101** and **LS102** with different additional acceptors BT and DFBT, respectively, for applications in DSSCs. In terms of induction effect, fluorine atoms are strong electron-withdrawing groups. However, this influence was suppressed by the electron-donating capacity of the conjugation effect from fluorine atoms, which impaired the electron-withdrawing ability of additional acceptor DFBT, resulting in **LS102** having a broader band gap and narrower UV-vis absorption spectrum. Along with the weaker dye loading capacity, the devices based on **LS102** had a lower J_{sc} (13.4 mA cm^{-2}) than that of **LS101** (15.1 mA cm^{-2}). The **LS102**-based DSSCs showed a V_{oc} of only 934 mV, compared with 966 mV for **LS101**, which was in agreement with the lower electron recombination resistance and chemical capacitance and shorter electron lifetime. The best PCEs achieved were 10.2% for **LS101** and 8.6% for **LS102**. Although DFBT showed excellent photovoltaic performance in polymer solar cells and SMOSCs, this rule was not applicable to DSSCs. Improved efficiency is only possible if the properties of the molecule and the solar cell are well matched.

Conflicts of interest

There are no conflicts of interest to declare.

References

1 M. Grätzel, *J. Photochem. Photobiol., C*, 2003, **4**, 145–153.
2 M. Grätzel, *J. Photochem. Photobiol., A*, 2004, **164**, 3–14.
3 H. Tan, C. Pan, G. Wang, Y. Wu, Y. Zhang, Y. Zou, G. Yu and M. Zhang, *Org. Electron.*, 2013, **14**, 2795–2801.
4 M. Freitag, J. Teuscher, Y. Saygili, X. Zhang, F. Giordano, P. Liska, J. Hua, S. M. Zakeeruddin, J.-E. Moser, M. Gratzel and A. Hagfeldt, *Nat. Photonics*, 2017, **11**, 372–378.
5 Y. S. Tingare, S. V. Nguyen, H.-H. Chou, Y.-C. Liu, Y.-S. Long, T.-C. Wu, T.-C. Wei and C.-Y. Yeh, *Adv. Energy Mater.*, 2017, **7**, 11.
6 L. Kavan, *Curr. Opin. Electrochem.*, 2017, **2**, 88–96.
7 Y. Ren, D. Sun, Y. Cao, H. N. Tsao, Y. Yuan, S. M. Zakeeruddin, P. Wang and M. Gratzel, *J. Am. Chem. Soc.*, 2018, **140**, 2405–2408.
8 S. Soman, S. C. Pradhan, M. Yoosuf, M. V. Vinayak, S. Lingamoorthy and K. R. Gopidas, *J. Phys. Chem. C*, 2018, **122**, 14113–14127.
9 B. O'Regan and M. Grätzel, *Nature*, 1991, **353**, 737–740.
10 Y. Xie, Y. Tang, W. Wu, Y. Wang, J. Liu, X. Li, H. Tian and W.-H. Zhu, *J. Am. Chem. Soc.*, 2015, **137**, 14055–14058.
11 Z. Yao, M. Zhang, H. Wu, L. Yang, R. Li and P. Wang, *J. Am. Chem. Soc.*, 2015, **137**, 3799–3802.
12 Y. K. Eom, S. H. Kang, I. T. Choi, Y. Yoo, J. Kim and H. K. Kim, *J. Mater. Chem. A*, 2017, **5**, 2297–2308.
13 W. Zhang, Y. Wu, H. W. Bahng, Y. Cao, C. Yi, Y. Saygili, J. Luo, Y. Liu, L. Kavan, J.-E. Moser, A. Hagfeldt, H. Tian, S. M. Zakeeruddin, W.-H. Zhu and M. Gratzel, *Energy Environ. Sci.*, 2018, **11**, 1779–1787.
14 K. Kakiage, Y. Aoyama, T. Yano, K. Oya, J.-i. Fujisawa and M. Hanaya, *Chem. Commun.*, 2015, **51**, 15894–15897.
15 S. Ahmad, E. Guillen, L. Kavan, M. Graetzel and M. K. Nazeeruddin, *Energy Environ. Sci.*, 2013, **6**, 3439–3466.
16 S. Kim, J. K. Lee, S. O. Kang, J. Ko, J. H. Yum, S. Fantacci, F. De Angelis, D. Di Censo, M. K. Nazeeruddin and M. Grätzel, *J. Am. Chem. Soc.*, 2006, **128**, 16701–16707.
17 L. Zhang, X. Yang, W. Wang, G. G. Gurzadyan, J. Li, X. Li, J. An, Z. Yu, H. Wang, B. Cai, A. Hagfeldt and L. Sun, *ACS Energy Lett.*, 2019, **4**, 943–951.
18 J. Wang, S. Liu, Z. Chai, K. Chang, M. Fang, M. Han, Y. Wang, S. Li, H. Han, Q. Li and Z. Li, *J. Mater. Chem. A*, 2018, **6**, 22256–22265.
19 J.-M. Ji, S. H. Kim, H. Zhou, C. H. Kim and H. K. Kim, *ACS Appl. Mater. Interfaces*, 2019, **11**, 24067–24077.
20 X. Gong, G. Li, Y. Wu, J. Zhang, S. Feng, Y. Liu, C. Li, W. Ma and Z. Bo, *ACS Appl. Mater. Interfaces*, 2017, **9**, 24020–24026.
21 H. Medlej, A. Nourdine, H. Awada, M. Abbas, C. Dagron-Lartigau, G. Wantz and L. Flandin, *Eur. Polym. J.*, 2014, **59**, 25–35.

22 A. C. Stuart, J. R. Tumbleston, H. Zhou, W. Li, S. Liu, H. Ade and W. You, *J. Am. Chem. Soc.*, 2013, **135**, 1806–1815.

23 Y.-X. Xu, C.-C. Chueh, H.-L. Yip, F.-Z. Ding, Y.-X. Li, C.-Z. Li, X. Li, W.-C. Chen and A. K. Y. Jen, *Adv. Mater. (Weinheim, Ger.)*, 2012, **24**, 6356–6361.

24 Y. Zhang, S.-C. Chien, K.-S. Chen, H.-L. Yip, Y. Sun, J. A. Davies, F.-C. Chen and A. K. Y. Jen, *Chem. Commun.*, 2011, **47**, 11026–11028.

25 H. Zhou, L. Yang, A. C. Stuart, S. C. Price, S. Liu and W. You, *Angew. Chem., Int. Ed.*, 2011, **50**, 2995–2998.

26 C.-Y. Chang, L. Zuo, H.-L. Yip, Y. Li, C.-Z. Li, C.-S. Hsu, Y.-J. Cheng, H. Chen and A. K. Y. Jen, *Adv. Funct. Mater.*, 2013, **23**, 5084–5090.

27 Y. Liang, Z. Xu, J. Xia, S.-T. Tsai, Y. Wu, G. Li, C. Ray and L. Yu, *Adv. Mater. (Weinheim, Ger.)*, 2010, **22**, E135–E138.

28 H. Bronstein, J. M. Frost, A. Hadipour, Y. Kim, C. B. Nielsen, R. S. Ashraf, B. P. Rand, S. Watkins and I. McCulloch, *Chem. Mater.*, 2013, **25**, 277–285.

29 S. Albrecht, S. Janietz, W. Schindler, J. Frisch, J. Kurpiers, J. Kniepert, S. Inal, P. Pingel, K. Fostiropoulos, N. Koch and D. Neher, *J. Am. Chem. Soc.*, 2012, **134**, 14932–14944.

30 N. Cho, K. Song, J. K. Lee and J. Ko, *Chem. - Eur. J.*, 2012, **18**, 11433–11439.

31 S. Li, X. Yang, D. Qu, W. Wang, Y. Wang and L. Sun, *Chin. J. Chem.*, 2012, **30**, 2315–2321.

32 X. Lu, X. Jia, Z.-S. Wang and G. Zhou, *J. Mater. Chem. A*, 2013, **1**, 9697–9706.

33 Y. Wu, W.-H. Zhu, S. M. Zakeeruddin and M. Grätzel, *ACS Appl. Mater. Interfaces*, 2015, **7**, 9307–9318.

34 P. Brogdon, H. Cheema and J. H. Delcamp, *ChemSusChem*, 2017, **10**, 3624–3631.

35 T. Marinado, K. Nonomura, J. Nissfolk, M. K. Karlsson, D. P. Hagberg, L. Sun, S. Mori and A. Hagfeldt, *Langmuir*, 2010, **26**, 2592–2598.

36 J. Bisquert, *Phys. Chem. Chem. Phys.*, 2003, **5**, 5360–5364.

37 K. D. Seo, B. S. You, I. T. Choi, M. J. Ju, M. You, H. S. Kang and H. K. Kim, *J. Mater. Chem. A*, 2013, **1**, 9947–9953.

38 J. N. Clifford, E. Martinez-Ferrero and E. Palomares, *J. Mater. Chem.*, 2012, **22**, 12415–12422.

39 M.-L. Han, Y.-Z. Zhu, S. Liu, Q.-L. Liu, D. Ye, B. Wang and J.-Y. Zheng, *J. Power Sources*, 2018, **387**, 117–125.

40 X. Song, X. Yang, H. Wang, J. An, Z. Yu, X. Wang, A. Hagfeldt and L. Sun, *Sol. Energy*, 2019, **187**, 274–280.